

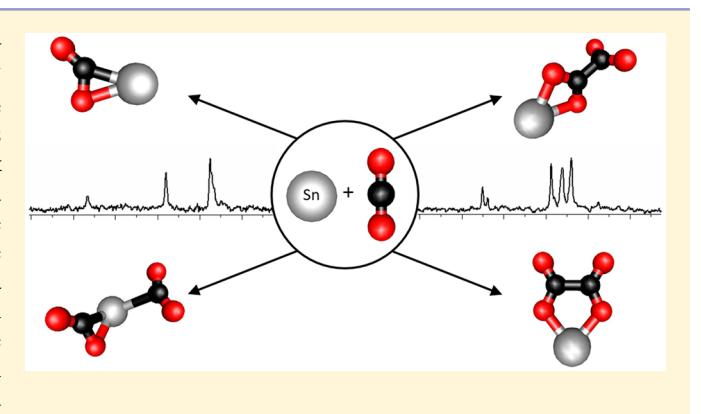
# Infrared Photodissociation Spectra of $[Sn(CO_2)_n]^-$ Cluster lons

Michael C. Thompson and J. Mathias Weber\*

JILA and Department of Chemistry and Biochemistry, University of Colorado, 440 UCB, Boulder, Colorado 80309-0440, United States

Supporting Information

ABSTRACT: We present infrared spectra and density functional theory calculations of mass selected  $[Sn(CO_2)_n]^{-1}$ cluster anions (n = 2-6). The spectra and structures of these clusters exhibit less structural diversity than those of analogous clusters with first-row transition metals, but are more complex than those for the heavy coinage metals or for the related  $[Bi(CO_2)_n]^-$  clusters. The most favorable core ion structure for all cluster sizes can be characterized as a Sn-oxalate complex,  $Sn[C_2O_4]^-$ . Higher energy isomers based on a bidentate  $\eta^2$ -(C,O) CO<sub>2</sub> ligand tightly bound to the metal atom in SnCO<sub>2</sub><sup>-</sup> complexes are also observed, even for the largest cluster sizes studied here. For n = 2, another high energy isomer is found, featuring a CO2 ligand weakly bound to the metal atom in a SnCO<sub>2</sub> ion.



## INTRODUCTION

The heterogeneous catalysis of CO<sub>2</sub> reduction on metal surfaces has been a topic of intense research over the past decades. Increased attention has been given to alternatives to the often employed noble and platinum group metals, as part of an effort to achieve reduction using less expensive and more abundant metals. Devices based on such metals, should they prove to be as efficient as traditional catalyst materials (or even better), would represent an industrially viable route toward a carbon neutral fuel cycle. Initial studies of electroreduction of CO<sub>2</sub> over post-transition metals (Bi, Sn, Pb) by Hori and coworkers in a low concentration solution of bicarbonate showed a preference for formic acid formation over the normally desired carbon monoxide products.<sup>2,3</sup> Additional studies investigating the reaction of CO2 with Sn nanoparticles suggest the generation of formate to be the dominant product under bicarbonate.4,5

In contrast, recent work by Rosenthal and co-workers, using electrochemically roughened post-transition metal surfaces in concert with ionic liquid solvents, has yielded several devices with Faradaic efficiencies toward CO formation that rival more expensive, traditional electrode materials (Ag, Au).<sup>6-8</sup>

While electrochemical experiments are useful in identifying viable catalyst materials and product distributions of CO2 reduction under different conditions, the fundamental interactions of the CO<sub>2</sub> species with electrode surfaces are not well understood. Experiments by Kanan and co-workers have shown that electrochemically roughened, nanoparticulate electrode surfaces exhibit higher Faradaic efficiencies than atomically flat surfaces.4,9,10

The details of molecular interactions with catalysts are difficult to study in situ (and even more difficult in operando) because of the complexity of a condensed phase environment. Negatively charged clusters of metal atoms with CO<sub>2</sub> can be used as well defined model systems to study the interaction of CO<sub>2</sub> with a metal atom in the presence of an excess electron, without suffering from such complexity. The geometry, vibrational frequencies, and charge distributions of these metal-CO<sub>2</sub> complexes provide fundamental insight into the interaction of CO2 with an undercoordinated, charged corner site on a nanoparticle or electrode surface. In this work, we present infrared photodissociation spectra of  $[Sn(CO_2)_n]^-$  (n =2-6) compared to calculated vibrational frequencies.

## METHODS

Experiments were performed using a home-built photodissociation spectrometer that has been described in detail previously. 11 Material from a rotating Sn target was vaporized by the third harmonic of a pulsed Nd:YAG laser (355 nm; 40 mJ/pulse; 5-7 ns pulse duration). The resulting metal vapor was then entrained into a pulsed supersonic expansion of CO<sub>2</sub> (550 kPa) generated with an Even-Lavie valve. The resulting anions were accelerated to ca. 3.5 keV kinetic energy in a custom Wiley-McLaren time-of-flight mass spectrometer. Mass selection of the target species of composition [Sn(CO<sub>2</sub>)<sub>n</sub>] was achieved using a pulsed mass gate located in the first space focus of the instrument. Mass selected ions were irradiated in a multipass cell<sup>12</sup> with the output of an infrared optical parametric converter system. Absorption of an infrared photon of sufficient energy by  $[Sn(CO_2)_n]^-$  clusters

Received: January 11, 2018 Revised: March 8, 2018 Published: March 29, 2018

resulted in the evaporation of a weakly bound  $\mathrm{CO}_2$  molecule from the cluster. The resulting change in ion mass was measured using a reflectron in a secondary mass analysis step. Photodissociation action spectra were generated by monitoring the formation of fragment ions as a function of photon energy, corrected for photon fluence. The experiment operates in the single-photon regime, as our pulse energies are insufficient for multiphoton processes to occur. Several spectra for each cluster size were measured on different days to ensure reproducibility and increase the signal-to-noise ratio. The experiment was operated at 20 Hz repetition rate.

The experimental spectra are presented in separate regions, corresponding to two different crystal settings of the light source. Since there are no spectroscopic features connecting the two regions, we cannot give exact relative intensities for the two different spectral regions. Instead, each spectrum is individually normalized to the highest intensity spectral feature and each region is normalized separately.

Quantum chemical calculations were performed using the TURBOMOLE suite of programs. 13 Cluster structures were optimized using density functional theory 14 (B3LYP functional)<sup>15</sup> with dispersion correction,<sup>16</sup> and def2-TZVPP<sup>17</sup> basis sets were used for all atoms. This basis set includes an ECP-28 effective core potential for the Sn atom to account for scalar relativistic effects. This level of theory has been successfully used in past work on metal-CO<sub>2</sub> anionic clusters. 18-Harmonic vibrational analysis was performed using the AOFORCE program,<sup>27</sup> and atomic charges were calculated employing natural population analysis.<sup>28</sup> Harmonic frequencies were scaled to account for anharmonicity, using a value of 0.975 based on a comparison of experimental and calculated frequencies for neutral CO2. A scaling factor of 0.9380 based on previous work<sup>29</sup> was used for the asymmetric stretching motion of carboxylate type ligands. Simulated spectra were generated by convoluting calculated frequencies and intensities with a Gaussian whose width corresponds to typically observed experimental peak widths (12 cm<sup>-1</sup> full width at halfmaximum). The  $[Sn(CO_2)_2]^-$  potential energy curve along the Sn-C stretching coordinate was generated using the same functional, and zero point energy contributions for this curve were included for all modes except for the Sn-C stretching mode.

# RESULTS AND DISCUSSION

**Overview.** Experimental spectra for  $[Sn(CO_2)_n]^-$  (n=2-6) are shown in Figure 1. Typically, vibrational modes that occur in the region from 1000 to 2150 cm<sup>-1</sup> are mostly localized on the negatively charged core ion, while transitions in the higher energy region are assigned to the antisymmetric stretching modes of  $CO_2$  molecules acting as solvent species.<sup>30</sup> The signatures in the solvent stretching region shift to the blue with increasing cluster size (ca. 3 cm<sup>-1</sup> per additional  $CO_2$  unit). This has been observed previously in other metal  $CO_2$  anionic cluster systems and can be explained with a diminishing influence of the molecular anion on each individual solvent species as the number of solvent molecules increases.<sup>18–26</sup>

Vibrational motions of the core ion can be characterized as asymmetric and symmetric stretching motions of carbon dioxide ligands bound to the metal atom. These ligands are often strongly reduced, which results in an average of the red shift of the symmetric and antisymmetric stretching frequencies compared to neutral CO<sub>2</sub>. Such shifts can be associated with the population of an antibonding orbital in the CO<sub>2</sub> unit, which

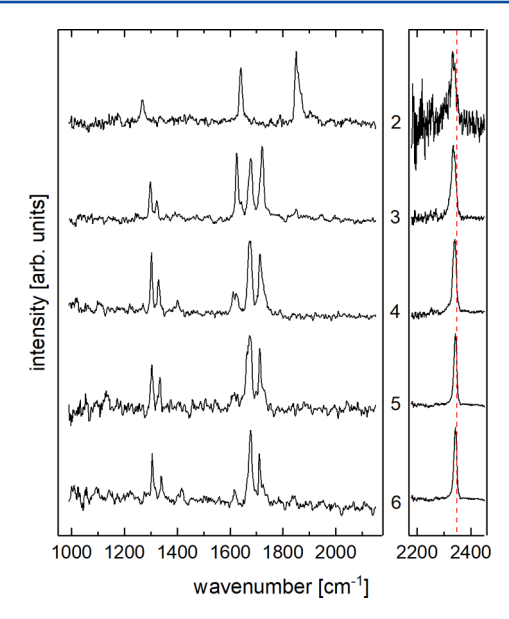


**Figure 1.** IR photodissociation spectra of  $[Sn(CO_2)_n]^-$  (n = 2-6). The numbers between the panels indicate the cluster size n. The traces in the two spectral regions are individually normalized to the most intense peak. The red dashed vertical line gives the position of the antisymmetric stretching mode of free  $CO_2$ .

results in an increase in the CO bond distance, diminishing CO bond strength, and a substantial deviation of the OCO bond angle from  $180^{\circ}.^{31,32}$ 

We note that there is an abrupt change in the lower energy region of the spectra from n = 2 to n = 3 where an intense feature at  $1850 \text{ cm}^{-1}$  (observed for n = 2) disappears, and two new spectral features emerge (for  $n \ge 3$ ) around 1680 and  $1720 \text{ cm}^{-1}$ . This suggests a change of the core ion structure that is the main contributor to the spectrum, and possibly its size. For clusters beyond n = 3, there are only small changes in peak positions, and no further evolution of the spectroscopic pattern but the relative intensities of some of the features change.

As stated above, the experimental spectra are collected as vibrational predissociation action spectra by monitoring the photon-induced generation of fragment ions as a function of photon energy. The detection efficiency in photodissociation spectroscopy generally depends on the magnitude of the binding energy of the most weakly bound species in the cluster compared to the photon energy. If this binding energy is significantly higher than the energy of a particular vibrational transition, photon-induced dissociation may still occur, as the residual energy in the cluster prior to irradiation combined with the photon energy can still suffice to lead to dissociation. The total thermal energy content of the clusters can be estimated assuming that they can be described as an evaporative ensemble, where the internal energy content of the cluster is estimated to be on the order of the binding energy of the last species to evaporate from it in the cluster source.<sup>33</sup> If the binding energy of the solvent species is higher than the incident photon energy, the probability for dissociation during the window of observation in the experiment (ca. 20  $\mu$ s) will be less than unity. This results in a suppression of the experimentally observed intensity of any mode whose energy is lower than the binding energy of the most weakly bound constituent of the cluster. Our calculations indicate that the solvent binding energies of Sn-CO<sub>2</sub> clusters depend on the core ion geometry as well as the solvation position, particularly for small clusters,

and are typically equivalent to ca. 1500 cm<sup>-1</sup>. Features below 1500 cm<sup>-1</sup> can therefore be expected to be weaker than in the predicted spectra.

 $[Sn(CO_2)_n]^-$  cluster ions can in principle occur in doublet or quartet spin states. The calculated energies for  $[Sn(CO_2)_n]^{-1}$ ions with doublet spin were lower in energy than those for ions with quartet spin by 100-300 kJ/mol, depending on the core ion geometry. Also, many structures that are stable in doublet spin configurations and are clearly identified in the spectra (see below) dissociate into a Sn anion and CO2 solvent species when calculated as a quartet species. The interaction between the Sn atom and the CO2 ligands is likely strong enough to break the symmetry of the 5p orbitals on the metal. This allows the doublet states to become more stable than the quartet states, even though the bare Sn anion has a quartet configuration. This finding is reminiscent of work on  $\operatorname{Sn}_{\frac{1}{4}}$ cluster anions. While atomic Sn has a quartet ground state, the dimer Sn<sub>2</sub><sup>-</sup> has a doublet ground state, 35 as do the larger clusters.<sup>36</sup> We note, however, that the infrared spectra do not allow us to unambiguously determine the spin state of the species studied here.

[Sn(CO<sub>2</sub>)<sub>2</sub>]<sup>-</sup>. The experimental spectrum of  $[Sn(CO<sub>2</sub>)_2]^-$  shows a high intensity feature at 1850 cm<sup>-1</sup>. An additional strong transition is found at 1640 cm<sup>-1</sup>. There is also a lower intensity feature at 1269 cm<sup>-1</sup> and a very weak signature at 1178 cm<sup>-1</sup>. In addition to the features in the core ion region, there is a peak at 2333 cm<sup>-1</sup>, which indicates that some of the clusters in the ion beam must be composed of a  $SnCO<sub>2</sub>^-$  core ion and one solvent molecule.

The experimental spectrum of  $[Sn(CO_2)_2]^-$  is presented along with several calculated structures in Figure 2, and the relative energies of these isomers (and others) are collected in Figure 3. The lowest energy isomer (A) at this cluster size has the two  $CO_2$  units forming an oxalato ligand, where the Sn atom is found bridging the two  $COO^-$  groups of the ligand, forming an overall planar structure. The next higher energy isomer (B) consists of a nonplanar oxalato ligand, binding to

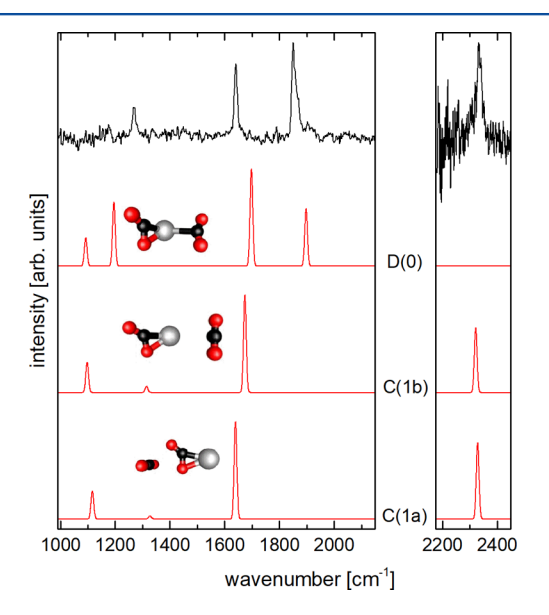


**Figure 2.** Calculated vibrational spectra of relevant structures of  $[Sn(CO_2)_2]^-$  (lower traces) compared to the experimental spectrum (upper trace). The nomenclature of the structures is explained in Figure 3. We estimate that the band at 2333 cm<sup>-1</sup> is a factor of 6–10 weaker than the band at 1850 cm<sup>-1</sup> (see text).

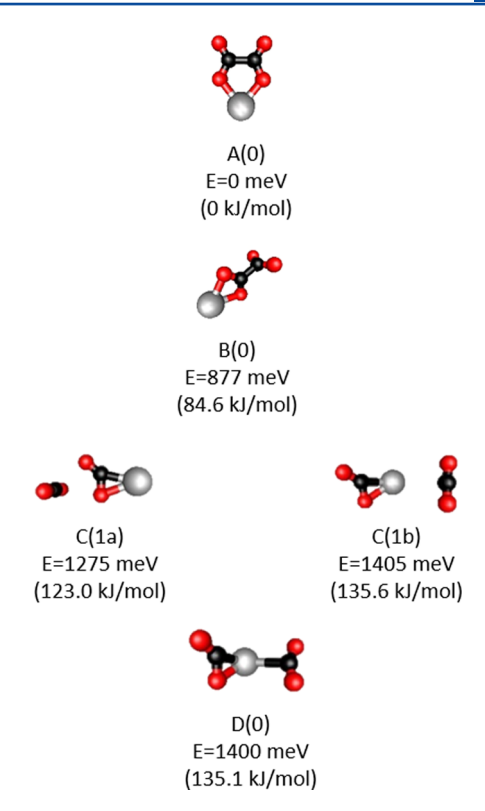


Figure 3. Minimum energy structures for  $[Sn(CO_2)_2]^-$ . Capital letters denote the core ion structure, and numbers and lower case letters in parentheses denote the number and position conformer of solvent species. No other minimum energy structures containing a solvent  $CO_2$  molecule were found at this cluster size regarding core ions or solvent isomers. Sn atoms are shown in gray, C atoms in black, and O atoms in red.

the Sn atom with both O atoms of one of its  $COO^-$  groups. Oxalato ligands are very common in metal— $CO_2$  cluster anions, and often form the lowest energy isomers in such systems.  $^{20,21,24-26}$ 

Since our detection scheme relies on the presence of weakly bound cluster constituents, with dissociation energies of the order of the photon energy, we can safely exclude core ion isomers A and B as sources of the observed spectrum for n = 2, since their binding energies are much higher than the photon energies (of the order of 100 kJ/mol and higher). While we assume that these low energy isomers are in fact present in the beam, they are unobservable by single photon infrared photodissociation spectroscopy, and we will discuss them for larger cluster sizes (see below). We restrict our discussion of the spectrum for n = 2 to those species that can dissociate upon absorption of a single photon in this spectral region. Core ions C and D fulfill this condition, although they are relatively high in energy. Freezing out higher energy isomers during cluster formation has been observed in many other metal— $CO_2$  cluster systems. <sup>20,21,24,25</sup> The assignments made in the following discussion are summarized in Table 1.

Both core ions C and D exhibit a  $CO_2$  ligand bound to the metal through its carbon and one oxygen atom. This  $\eta^2$ -(C,O) binding motif has been found previously in several other metal— $CO_2$  cluster anions and is one of the most common metal— $CO_2$  ligand binding motifs. On the basis of the calculated vibrational frequencies, we assign the transition at 1640 cm<sup>-1</sup> to the asymmetric stretching frequency of such a bidentate  $CO_2$  ligand. The symmetric stretching mode of this

Table 1. Assignments for the Spectrum at n = 2

	$\begin{array}{c} observed \\ (cm^{-1}) \end{array}$	mainly contributing core ion and vibrational mode	$\begin{array}{c} predicted \\ (cm^{-1}) \end{array}$	
	1178	D, symmetric CO stretch of $\eta^2$ -(C,O) ligand	1092	
	1269	D, symmetric carboxylate CO stretch	1196	
	1640	D, asymmetric CO stretch of $\eta^2$ -(C,O) ligand	1698	
	1850	D, antisymmetric carboxylate CO stretch	1898	
	2333	C, antisymmetric CO stretch of solvent	2326 <sup>a</sup>	
<sup>a</sup> Average value of isomers C(1a) and C(1b).				

ligand is predicted to appear around 1100 cm<sup>-1</sup> and is likely the cause of the very weak feature observed at 1178 cm<sup>-1</sup>.

The comparison of experimental and calculated spectra suggests that the main contribution to the observed spectrum comes from core ion structure D, which does not allow for the presence of a solvent molecule at this cluster size. This is consistent with the low signal-to-noise ratio of the feature in the solvent region, indicating that only a very small fraction of the ions contributing to the spectrum contains a solvent molecule. While we cannot directly compare relative intensities for the two different spectral regions (see the Methods section), we estimate that the band at 2333 cm<sup>-1</sup> is a factor of 6–10 weaker than the band at 1850 cm<sup>-1</sup>. As a result, we cannot observe the features belonging to core ion structure C in the core ion region.

Core ion isomer D features an  $\eta^2$ -(C,O) ligand as well as a second ligand that is bound through the carbon atom of the CO<sub>2</sub> species. This  $\eta^1$ -C metalloformate binding motif has been observed previously in other gas phase metal CO<sub>2</sub> cluster anions. <sup>22,23,26</sup> The calculated bond dissociation energy of the  $\eta^1$ -C ligand predicts the Sn–C bond strength to be around 1500 cm<sup>-1</sup>, suggesting that it can be broken by the absorption of a single photon in the experimentally relevant spectral region. As explained above, the features at lower frequencies will be suppressed and appear only because dissociation is assisted by the thermal energy content imparted on the ion in the ion source.

In the  $\eta^1$ -C binding motif, the electrophilic carbon atom of the CO<sub>2</sub> molecule interacts with a partially negatively charged metal atom, in this case the Sn atom. Electrophilic attack at the metal atom results in a donation of charge from the  $\eta^2$ -(C,O) complex into the carboxylate group. Charge donation into this second CO<sub>2</sub> ligand results in a red shift of the asymmetric CO stretching frequency of that ligand. On the basis of the calculated spectra, it is straightforward to assign the high intensity transition at 1850 cm<sup>-1</sup> to the antisymmetric CO stretching mode of the carboxylate ligand. The symmetric stretching mode of the carboxylate ligand is calculated to be at 1194 cm<sup>-1</sup>, and can be assigned to the experimental feature at 1269 cm<sup>-1</sup>. The asymmetric stretching motion of the  $\eta^2$ -(C,O) ligand can be assigned to the experimental transition at 1640 cm<sup>-1</sup>.

As mentioned above, the presence of a solvent signature implies the presence of clusters containing a  $SnCO_2^-$  core ion and a solvent molecule. Structures C(1a) and C(1b) feature a single, strongly bound  $\eta^2$ -(C,O) ligand and a solvent molecule. Core ion C may contribute to the spectroscopic feature at 1640 cm<sup>-1</sup>. However, core ions C and D are predicted to have signatures that differ by ca. 25 cm<sup>-1</sup> in this region. Since the relative abundance of core ion C is likely to be small compared to that of core ion D, and the observed peak at 1640 cm<sup>-1</sup> is

narrower than the predicted difference of the two signatures (the full width at half-maximum is 14 cm<sup>-1</sup>), we assign this feature to core ion D. The only clear proof of the existence of core ion C is the feature in the solvent region at 2333 cm<sup>-1</sup>.

Interestingly, isomers C(1b) and D(0) are structurally very similar, and represent two minima on a potential energy surface, describing physisorbed and chemisorbed  $CO_2$  on a  $SnCO_2^-$  core ion, respectively (see Figure 4). Transformation

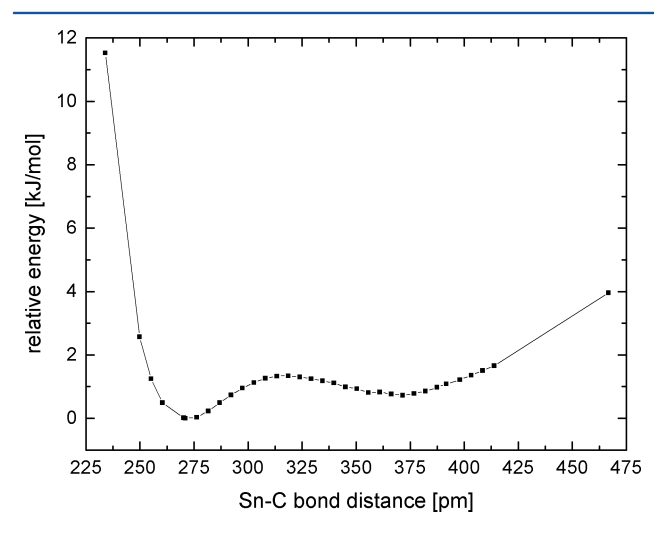


Figure 4. Calculated potential energy surface of structure D(0) along the Sn-C bond distance coordinate; all other coordinates were allowed to relax. Energies are corrected for zero point energy along all modes except for the Sn-C stretching mode.

of C(1b) into D(0) occurs by the formation of a Sn–C bond. The highest occupied molecular orbital (HOMO) provides insight into the interaction between the Sn atom and  $CO_2$  ligand. A comparison of the HOMOs of structures C(1b) and D(0) along with the transition state is shown in Figure 5. In the

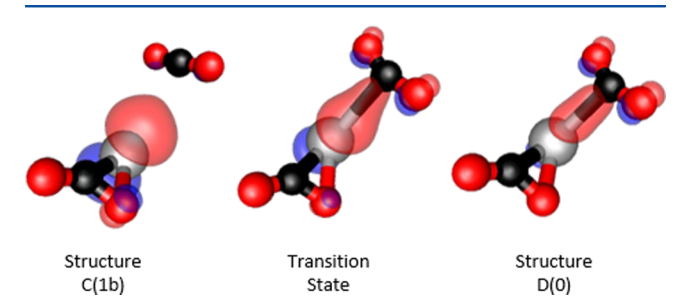


Figure 5. HOMO contours of several structures along the Sn–C bond length potential energy surface connecting structures C(1b), left, and D(0), right. Isosurfaces shown are at 70% of the maximum orbital amplitude.

case of structure D(0), one of the p-orbitals of the Sn atom is mixing with one of the  $\pi$  orbitals of the carboxylic  $CO_2$  ligand. Calculated atomic charges suggest that this bond results in a transfer of -0.41 e of charge onto the  $\eta^1$ -C ligand. Most of this charge is transferred out of the Sn atom, which is neutral in structure C(1b) but has a charge of +0.35 e in structure D(0). We note that along this potential energy surface there are no rapid changes in either the C-O bond distances or the OCO bond angle of the carboxylate ligand, suggesting a gradual change in the character of the second  $CO_2$  molecule from solvent to ligand. This is reflected in a gradual elongation of the

Sn p-orbital, eventually forming a weak  $\sigma$ -bond with the CO<sub>2</sub> ligand. The existence of both a chemisorbed and a physisorbed isomer, their potential energy minima separated only by a difference in the metal–carbon distance, has been found in gold–CO<sub>2</sub> complex anions, even though the experimental record has been ambiguous for these species. <sup>29,37,38</sup>

The present case shows experimental evidence for both types of complexes, where the binding partner for the chemisorbed/ physisorbed CO<sub>2</sub> unit is a [SnCO<sub>2</sub>]<sup>-</sup> complex. While the calculated potential energy surface seems to show a route for direct interconversion between a chemisorbed and a physisorbed CO2 molecule, we note that the surface shown in Figure 4 is questionable regarding the barrier height, and even regarding the existence of a local minimum corresponding to the physisorbed structure C(1b). The calculated barrier to Sn-C bond formation starting from isomer C(1b) is only around 0.6 kJ/mol. This suggest that the cluster is very floppy, with rapid interconversion between structure D(0) and structure C(1b). However, the calculated spectrum for the (static) structure D(0) fits very well to the experimental signatures. One would expect broad intermediate spectroscopic features if rapid interconversion between the two structures were to occur, but these are not reflected in the experimental spectrum. We therefore assume that either the barrier height is underestimated by our calculations or the physisorbed structure C(1b) does not exist. In the latter case, the solvent signature at 2333 cm<sup>-1</sup> would be caused solely by isomer C(1a).

In comparison to other metalloformate species, the  $[Sn(CO_2)_2]^-$  system is unique due to the low bond dissociation energy of the Sn–C bond. While similar experiments<sup>29</sup> on AuCO<sub>2</sub><sup>-</sup> (calculated bond dissociation energy ca. 33 kJ/mol) needed two infrared photons for dissociation, the calculated dissociation energy in the present work (ca. 18 kJ/mol) and the much better signal-to-noise ratio compared to ref 29 strongly suggest that dissociation of  $[Sn(CO_2)_2]^-$ , while it may be thermally assisted, occurs upon absorption of a single infrared photon.

As mentioned above, it is important to note that the infrared spectrum for n=2 likely does not encode the dominant core ion geometry at this cluster size, since the lowest energy structures cannot dissociate upon absorption of a single infrared photon. However, the spectrum allows insight into the structural behavior of higher energy isomers, which are of fundamental interest in the context of other metal— $CO_2$  complexes and their chemical bonding.

 $[Sn(CO_2)_3]^-$ . Increasing the cluster size by an additional  $CO_2$ molecule results in a number of changes in the IR photodissociation spectrum compared to  $[Sn(CO_2)_2]^-$ . The experimental spectrum contains three strong features in the spectral region characteristic for the core ion signatures, with peaks at 1625, 1678, and 1721 cm<sup>-1</sup> as well as two lower intensity features at 1299 and 1323 cm<sup>-1</sup>. The most pronounced changes from n = 2 to n = 3 are the disappearance of the large spectral feature found at 1850 cm<sup>-1</sup> in the spectrum for n = 2, the change of the spectral signatures around 1700 cm<sup>-1</sup>, and the increase in the intensity of the solvent signature, reflected in its strongly increased signal-to-noise ratio. The increase of the intensity of the solvent feature indicates that, unlike in  $[Sn(CO_2)_2]^-$ , a significant part of the cluster ions have at least one solvent CO2 molecule. Calculated structures are provided in Figure 6, and a comparison of predicted spectra with the experimental spectrum is shown in Figure 7. Table 2 summarizes the assignments as discussed below.

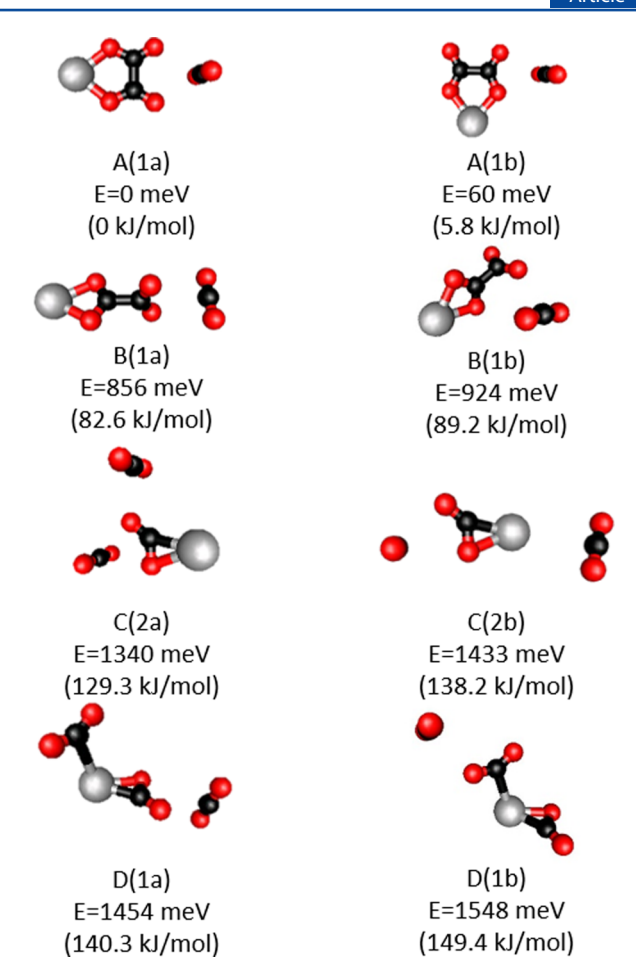


**Figure 6.** Calculated structures of  $[Sn(CO_2)_3]^-$  clusters. Structures are calculated in the doublet spin state, and all energies are relative to the lowest energy calculated structure at this size.

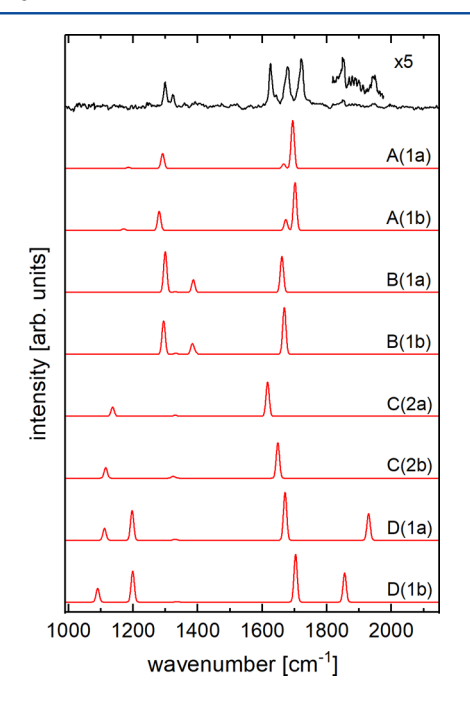


**Figure 7.** Calculated vibrational spectra of several conformers of  $[Sn(CO_2)_3]^-$  (red) compared to the experimental spectrum (black). A section of the experimental spectrum is enhanced to highlight low intensity features.

The Journal of Physical Chemistry A

Table 2. Assignments for the Spectrum at n = 3

observed (cm <sup>-1</sup> )	mainly contributing core ion and vibrational mode	predicted <sup>a</sup> (cm <sup>-1</sup> )
1299	A, in-phase combination of metal-bound CO stretches	1286
1323	B, out-of-phase combination of symmetric $CO_2$ stretches	1297
1625	C, asymmetric CO stretch, structure C(2a)	1616
1678	B, antisymmetric stretch of free CO <sub>2</sub> subunit	1664
1721	A, in-phase combination of free CO stretches	1698
1850	D, antisymmetric carboxylate CO stretch, structure $D(1b)$	1855
1945	D, antisymmetric carboxylate CO stretch, structure D(1a)	1929

"Unless assigned to specific solvent isomers, average values of different solvent isomers are reported.

The absence of any high intensity features in the region from 1800 to  $1900 \, \mathrm{cm^{-1}}$  for n=3 suggests that core ion geometry D does not significantly contribute to the photodissociation spectrum at this cluster size. There are, however, weak signatures at 1850 and  $1945 \, \mathrm{cm^{-1}}$ , which we assign to the antisymmetric CO stretching mode of the carboxylate ligand for different solvent conformers around core ion D, denoted D(1a) and D(1b) in Figures 6 and 7. The sensitivity of this feature to solvent position is consistent with this assignment, as demonstrated for other metalloformate complexes. The bidentate ligand of core ion D likely contributes to some of the signatures around  $1700 \, \mathrm{cm^{-1}}$ , but the weak intensity of its higher energy signatures indicates that it is not one of the main sources for these intense bands.

Solvation around core ion structure D results in a destabilization of the weak Sn-C bond, particularly for solvation around the bidentate CO<sub>2</sub> ligand, which polarizes electron density out of the carboxylate bound ligand. This destabilization ultimately favors core ion C, and the calculated energies for the isomers shown in Figure 6 corroborate this interpretation. Structures C(2a) and C(2b) feature two different solvation environments around the bidentate CO<sub>2</sub> ligand, one where both solvent molecules are on the ligand side of the complex and another where there is a solvent molecule on either side of the complex (see Figure 6). The solvation environment around the bidentate ligand of core ion C affects the frequency of the asymmetric CO<sub>2</sub> stretching mode. We assign the asymmetric CO stretching mode of structure C(2a) to the experimental feature at 1625 cm<sup>-1</sup>. Core ion C(2b) likely contributes to the peak at 1678 cm<sup>-1</sup>, although there are likely contributions to this peak from other core ion isomers, as discussed below.

The addition of a third CO<sub>2</sub> molecule to the cluster allows for core ion geometries featuring two CO<sub>2</sub> ligands to be solvated, making the signatures of core ion isomers A and B apparent in the experimental spectrum. For the description of the vibrations of core ion A, we characterize the normal modes of the oxalato ligand in terms of coupled metal-bound and free CO oscillators. The in-phase stretching motion of the free CO oscillators and the in-phase motion of the metal-bound CO oscillators each have a high oscillator strength, while the out-of-phase combinations are much weaker. We assign the transition at 1721 cm<sup>-1</sup> to the in-phase combination of the free CO oscillators in the planar oxalato ligand of core ion A, while the out-of-phase combination likely contributes to the peak at 1678 cm<sup>-1</sup>. The metal-bound CO oscillators are at lower frequencies

due to the weakening of the corresponding CO bonds by interaction with the metal, and we assign the feature at 1299 cm<sup>-1</sup> to the in-phase combination of the metal-bound CO oscillators of core ion A. The out-of-phase combination is predicted to carry only very little intensity, and we do not observe it in the spectrum. Different solvation positions do not result in strong differences in the vibrational signatures of core ion A.

Structural family B introduces a different connectivity of the Sn atom to the oxalato ligand, where the metal only interacts with a single  $\mathrm{CO}_2$  subunit. This interaction can be described as an extension of the  $\eta^2$ -(O,O) motif previously identified by Asmis and co-workers in MgCl-CO<sub>2</sub>-,<sup>39</sup> where the highly nucleophilic carbon atom of the carbene species has bonded with a second  $\mathrm{CO}_2$  unit, forming a C-C bond, and transferring electron density from the carbene ligand into the second  $\mathrm{CO}_2$  unit. Unlike in planar oxalate complexes, where the C-C torsion angle is locked due to interactions with the metal, structural family B features a staggered oxalato ligand, due to the repulsion of the partially negative oxygen atoms.

Different from core ion A, the CO<sub>2</sub> subunits in core ion structure B are no longer equivalent, leading to changes in the coupling of the CO stretching modes of the two subunits. The "free" CO2 subunit has a calculated OCO angle of 132° and a predicted asymmetric CO<sub>2</sub> vibrational frequency of 1664 cm<sup>-1</sup>. In contrast, the interaction of the metal with the oxygen atoms results in a calculated OCO bond angle of 116° for the metal bound CO<sub>2</sub> subunit and a strongly red-shifted asymmetric CO<sub>2</sub> vibrational frequency predicted at 1385 cm<sup>-1</sup>. This difference highlights the significant influence of the metal on the asymmetric CO<sub>2</sub> stretching frequency of the metal bound CO<sub>2</sub> subunit, even though the charges of the two CO<sub>2</sub> moieties are similar. We assign the experimental feature at 1678 cm<sup>-1</sup> to the asymmetric stretching motion of the "free" CO2 subunit of a nonplanar oxalate ligand. The asymmetric stretching mode of the metal-bound CO2 subunit is likely too weak to be observable at this cluster size, but a feature compatible with the predicted frequency position for this mode appears for larger clusters (see Figure 1). Unlike the asymmetric stretching modes, the symmetric stretching modes of the individual CO<sub>2</sub> subunits are strongly coupled, resulting in in-phase and out-ofphase combinations. We assign the out-of-phase combination of symmetric stretching motions of the individual CO<sub>2</sub> subunits to the peak at 1323 cm<sup>-1</sup>. The intensity of the in-phase combination (at 1331 cm<sup>-1</sup>) is predicted to be too weak to be observable in the current experiment. Different solvation positions do not strongly differ in the vibrational signatures for core ion B.

**Larger Cluster Sizes.** The size evolution of the experimental spectra can reveal whether core ion structures are stable under increased solvation, especially when considering small core ions. Since no new signatures appear in the spectrum at larger cluster sizes, we assume that no new core ion structures are established at increasing levels of solvation. The main change in the experimental spectrum as cluster size increases above n=3 is a loss of intensity in the asymmetric stretching mode assigned to core ion C. This suggests that increasing solvation results in isomerization into a different core ion, likely A or B. Structural family D is no longer significantly populated in the experiment for  $n \ge 3$ .

The observation of high energy isomers at all cluster sizes studied here implies that there are significant barriers to isomerization into the lowest energy core ion isomer (A),

resulting in ions that are kinetically trapped in high energy structures. This is a common theme in cluster anions of metal atoms with  $CO_2$ ,  $^{18-21,24,25}$  and  $[Sn(CO_2)_n]^-$  clusters are no exception. As an example, exploratory calculations allow us to estimate the barrier to conversion of core ion isomer B into core ion isomer A at ca. 70 kJ/mol, allowing this isomer to exist with significant abundance, despite its high energy.

## CONCLUSIONS

Infrared photodissociation spectroscopy of  $[Sn(CO_2)_n]^-$  cluster anions in concert with quantum chemical calculations reveals information regarding the interaction between  $CO_2$  and atomic Sn in the presence of an excess electron.

The smallest cluster for which an infrared photodissociation spectrum is observed (n=2) shows how a  $\mathrm{CO}_2$  molecule can undergo bonding to the Sn atom in a  $\mathrm{SnCO}_2^-$  ion, leading to a weakly bound carboxylate ligand, reminiscent of other metal— $\mathrm{CO}_2$  complexes. The spectrum therefore allows insight into interesting fundamental aspects of metal— $\mathrm{CO}_2$  bonding. However, the spectrum for n=2 is unlikely to encode the structures of the most prevalent core ions.

This changes for  $n \ge 3$ , where the spectrum likely does reflect the structures of the dominant core ions of the clusters. These can be characterized as tin-oxalato complexes, where the oxalato ligand can be coplanar with the tin atom, with the latter bridging the two  $CO_2$  subunits of the ligand. Another form identifiable in the spectrum for n = 3, and gaining in importance for larger clusters, is an oxalato ligand bound to the Sn atom with the two O atoms of one of its  $CO_2$  subunits. Finally, a single  $\eta^2$ -(C,O)  $CO_2$  ligand is also identifiable at n = 3 but becomes less important as solvation increases. Larger clusters clearly favor oxalato ligands over other interaction motifs. For all cluster sizes, high-energy core ion isomers are observed, reflecting the fact that barriers to isomerization are sufficiently high for these species to be kinetically trapped.

While nanocrystalline tin and bismuth electrodes show similar performance for the electrocatalytic reduction of  $CO_2$ , the interaction of  $CO_2$  with atomic tin is somewhat different than that of other metal atoms in negatively charged metal— $CO_2$  cluster ions, where the metal is a good electrocatalyst for  $CO_2$  reduction.  $^{22,23,26}$  In particular, small  $[Sn(CO_2)_n]^-$  cluster anions do not preferentially form metalloformate complexes, which have been identified in other cluster anions, and may be the basis for the functional interactions of electrocatalytically active metals with  $CO_2$ .

## ASSOCIATED CONTENT

## Supporting Information

The Supporting Information is available free of charge on the ACS Publications website at DOI: 10.1021/acs.jpca.8b00362.

Calculated structure coordinates, vibrational frequencies, and charges of  $[Sn(CO_2)_n]^-$  (n = 2, 3) (PDF)

# AUTHOR INFORMATION

## **Corresponding Author**

\*E-mail: weberjm@jila.colorado.edu. Phone: +1-303-492-7841.

## ORCID

J. Mathias Weber: 0000-0002-5493-5886

#### **Notes**

The authors declare no competing financial interest.

## ACKNOWLEDGMENTS

We gratefully acknowledge funding from the National Science Foundation (NSF) through the NSF AMO Physics Frontier Center at JILA (PHY-1125844 and PHY-1734006). We also acknowledge graduate student support from the U.S. Department of Education through a GAANN Fellowship for M.C.T.

## REFERENCES

- (1) Hori, Y. In *Modern Aspects of Electrochemistry*; Vayenas, C. G., White, R. E., Gamboa-Aldeco, M. E., Eds.; Springer: New York, 2008; pp 89–189.
- (2) Hori, Y.; Wakebe, H.; Tsukamoto, T.; Koga, O. Electrocatalytic process of CO selectivity in electrochemical reduction of CO<sub>2</sub> at metal electrodes in aqueous media. *Electrochim. Acta* **1994**, *39*, 1833–1839.
- (3) Yoshio,  $\overline{H_1}$ ; Katsuhei, K.; Shin, S. Production of CO and  $CH_4$  in electrochemical reduction of  $CO_2$  at metal electrodes in aqueous hydrogenearbonate solution. *Chem. Lett.* **1985**, *14*, 1695–1698.
- (4) Chen, Y.; Li, C. W.; Kanan, M. W. Aqueous CO<sub>2</sub> reduction at very low overpotential on oxide-derived Au nanoparticles. *J. Am. Chem. Soc.* **2012**, *134*, 19969–19972.
- (5) Del Castillo, A.; Alvarez-Guerra, M.; Irabien, A. Continuous electroreduction of CO<sub>2</sub> to formate using Sn gas diffusion electrodes. *AIChE J.* **2014**, *60*, 3557–3564.
- (6) Medina-Ramos, J.; Pupillo, R. C.; Keane, T. P.; DiMeglio, J. L.; Rosenthal, J. Efficient conversion of CO<sub>2</sub> to CO using tin and other inexpensive and easily prepared post-transition metal catalysts. *J. Am. Chem. Soc.* **2015**, *137*, 5021–5027.
- (7) Medina-Ramos, J.; DiMeglio, J. L.; Rosenthal, J. Efficient reduction of CO<sub>2</sub> to CO with high current density using in situ or ex situ prepared Bi-based materials. *J. Am. Chem. Soc.* **2014**, *136*, 8361–8367.
- (8) DiMeglio, J. L.; Rosenthal, J. Selective conversion of CO<sub>2</sub> to CO with high efficiency using an inexpensive bismuth-based electrocatalyst. *J. Am. Chem. Soc.* **2013**, *135*, 8798–8801.
- (9) Li, C. W.; Ciston, J.; Kanan, M. W. Electroreduction of carbon monoxide to liquid fuel on oxide-derived nanocrystalline copper. *Nature* **2014**, *508*, 504–507.
- (10) Li, C. W.; Kanan, M. W. CO<sub>2</sub> reduction at low overpotential on Cu electrodes resulting from the reduction of thick Cu<sub>2</sub>O films. *J. Am. Chem. Soc.* **2012**, *134*, 7231–7234.
- (11) Weber, J. M. A pulsed ion source for the preparation of metal containing cluster ions using supersonic entrainment of laser vaporized metal. *Rev. Sci. Instrum.* **2005**, *76*, 043301.
- (12) Riedel, J.; Yan, S. N.; Kawamata, H.; Liu, K. P. A simple yet effective multipass reflector for vibrational excitation in molecular beams. *Rev. Sci. Instrum.* **2008**, *79*, 033105.
- (13) Ahlrichs, R.; Bär, M.; Häser, M.; Horn, H.; Kölmel, C. Electronic-Structure Calculations on Workstation Computers the Program System Turbomole. *Chem. Phys. Lett.* **1989**, *162*, 165–169.
- (14) Lee, C. T.; Yang, W. T.; Parr, R. G. Development of the collesalvetti correlation-energy formula into a functional of the electron-density. *Phys. Rev. B: Condens. Matter Mater. Phys.* **1988**, *37*, 785–789.
- (15) Becke, A. D. Density-functional exchange-energy approximation with correct asymptotic-behavior. *Phys. Rev. A: At., Mol., Opt. Phys.* **1988**, 38, 3098–3100.
- (16) Grimme, S. Semiempirical GGA-type density functional constructed with a long-range dispersion correction. *J. Comput. Chem.* **2006**, 27, 1787–1799.
- (17) Weigend, F.; Ahlrichs, R. Balanced basis sets of split valence, triple zeta valence and quadruple zeta valence quality for H to Rn: Design and assessment of accuracy. *Phys. Chem. Chem. Phys.* **2005**, *7*, 3297–3305.
- (18) Knurr, B. J.; Weber, J. M. Structures of  $[CoO(CO_2)_n]^-$  and  $[NiO(CO_2)_n]^-$  clusters studied by infrared spectroscopy. *J. Phys. Chem. A* **2015**, *119*, 843–850.
- (19) Knurr, B. J.; Weber, J. M. Infrared spectra and structures of anionic complexes of cobalt with carbon dioxide ligands. *J. Phys. Chem.* A **2014**, *118*, 4056–4062.

- (20) Knurr, B. J.; Weber, J. M. Interaction of nickel with carbon dioxide in  $[Ni(CO_2)_n]^-$  clusters studied by infrared spectroscopy. *J. Phys. Chem. A* **2014**, *118*, 8753–8757.
- (21) Knurr, B. J.; Weber, J. M. Structural diversity of copper— $CO_2$  complexes: infrared spectra and structures of  $[Cu(CO_2)_n]^-$  clusters. *J. Phys. Chem. A* **2014**, *118*, 10246–10251.
- (22) Knurr, B. J.; Weber, J. M. Solvent-mediated reduction of carbon dioxide in anionic complexes with silver atoms. *J. Phys. Chem. A* **2013**, *117*, 10764–10771.
- (23) Knurr, B. J.; Weber, J. M. Solvent-driven reductive activation of carbon dioxide by gold anions. *J. Am. Chem. Soc.* **2012**, *134*, 18804–18808.
- (24) Thompson, M. C.; Dodson, L. G.; Weber, J. M. Structural motifs of  $[Fe(CO_2)_n]^-$  clusters (n = 3-7). *J. Phys. Chem. A* **2017**, 121, 4132–4138.
- (25) Thompson, M. C.; Ramsay, J.; Weber, J. M. Interaction of  $CO_2$  with atomic manganese in the presence of an excess negative charge probed by infrared spectroscopy of  $[Mn(CO_2)_n]^-$  clusters. J. Phys. Chem. A 2017, 121, 7534–7542.
- (26) Thompson, M. C.; Ramsay, J.; Weber, J. M. Solvent-driven reductive activation of CO<sub>2</sub> by bismuth: Switching from metalloformate complexes to oxalate products. *Angew. Chem., Int. Ed.* **2016**, *55*, 15171–15174.
- (27) Deglmann, P.; Furche, F.; Ahlrichs, R. An efficient implementation of second analytical derivatives for density functional methods. *Chem. Phys. Lett.* **2002**, *362*, 511–518.
- (28) Reed, A. E.; Weinstock, R. B.; Weinhold, F. Natural population analysis. *J. Chem. Phys.* **1985**, 83, 735–746.
- (29) Boese, A. D.; Schneider, H.; Gloess, A. N.; Weber, J. M. The infrared spectrum of Au CO<sub>2</sub>. *J. Chem. Phys.* **2005**, *122*, 154301.
- (30) Shin, J. W.; Hammer, N. I.; Johnson, M. A.; Schneider, H.; Glöss, A.; Weber, J. M. An infrared investigation of the  $(CO_2)_n$ -clusters: Core ion switching from both the ion and solvent perspectives. *J. Phys. Chem. A* **2005**, *109*, 3146–3152.
- (31) Walsh, A. D. 467. The electronic orbitals, shapes, and spectra of polyatomic molecules. Part II. Non-hydride AB<sub>2</sub> and BAC molecules. *J. Chem. Soc.* **1953**, 2266–2288.
- (32) Weber, J. M. The interaction of negative charge with carbon dioxide Insight into solvation, speciation and reductive activation from cluster studies. *Int. Rev. Phys. Chem.* **2014**, 33, 489–519.
- (33) Klots, C. E. Evaporative cooling. *J. Chem. Phys.* **1985**, 83, 5854–5860.
- (34) Miller, T. M.; Miller, A. E. S.; Lineberger, W. C. Electron affinities of Ge and Sn. *Phys. Rev. A: At., Mol., Opt. Phys.* **1986**, 33, 3558–3559.
- (35) Ho, J.; Polak, M. L.; Lineberger, W. C. Photoelectron spectroscopy of group IV heavy metal dimers: Sn<sup>-</sup>2, Pb<sup>-</sup>2, and SnPb<sup>-</sup>. *J. Chem. Phys.* **1992**, *96*, 144–154.
- (36) Moravec, V. D.; Klopcic, S. A.; Jarrold, C. C. Anion photoelectron spectroscopy of small tin clusters. *J. Chem. Phys.* **1999**, *110*, 5079–5088.
- (37) Kimble, M. L.; Castleman, A. W.; Mitrić, R.; Bürgel, C.; Bonačić-Koutecký, V. Reactivity of atomic gold anions toward oxygen and the oxidation of CO: Experiment and theory. *J. Am. Chem. Soc.* **2004**, *126*, 2526–2535.
- (38) Zhang, X.; Lim, E.; Kim, S. K.; Bowen, K. H. Photoelectron spectroscopic and computational study of  $(M-CO_2)^-$  anions, M=Cu, Ag, Au. *J. Chem. Phys.* **2015**, *143*, 174305.
- (39) Miller, G. B. S.; Esser, T. K.; Knorke, H.; Gewinner, S.; Schoellkopf, W.; Heine, N.; Asmis, K. R.; Uggerud, E. Spectroscopic identification of a bidentate binding motif in the anionic magnesium-CO<sub>2</sub> complex (ClMgCO<sub>2</sub>)<sup>-</sup>. *Angew. Chem., Int. Ed.* **2014**, 53, 14407–14410.